Soft Matter

PAPER

View Article Online
View Journal | View Issue

Cite this: *Soft Matter*, 2017, **13**, 2075

Nanotribological properties of nanostructured poly(cysteine methacrylate) brushes

Omed Al-Jaf,[a] Abdullah Alswieleh,[b] Steven P. Armes[a] and Graham J. Leggett*[a]

The nanomechanical properties of zwitterionic poly(cysteine methacrylate) (PCysMA) brushes grown from planar surfaces by atom transfer radical polymerisation have been characterised by friction force microscopy (FFM). FFM provides quantitative insights into polymer structure–property relationships and in particular illuminates the dependence of brush swelling on chain packing in nanostructured materials. In ethanol, which is a poor solvent for PCysMA, a linear friction–load relationship is observed, indicating that energy dissipation occurs primarily through ploughing. In contrast, in a good solvent for PCysMA such as water, a non-linear friction–load relationship is observed that can be fitted by Derjaguin–Muller–Toporov (DMT) mechanics, suggesting that the relatively small modulus of the swollen polymer leads to a large contact area and consequently a significant shear contribution to energy dissipation. The brush grafting density was varied by using UV photolysis of C–Br bonds at 244 nm to dehalogenate the surface in a controlled fashion. The surface shear strength increases initially as the brush grafting density is reduced, but then decreases for UV doses greater than 0.5 J cm^{-2}, reaching a limiting value when the brush thickness is *ca.* 50% that of a brush monolayer. Below this critical grafting density, a collapsed brush layer is obtained. For nm-scale gradient brush structures formed *via* interferometric lithography, the mean width increases as the period is increased, and the lateral mobility of brushes in these regions is reduced, leading to an increase in brush height as the grafted chains become progressively more extended. For a width of 260 nm, the mean brush height in water and ethanol is close to the thickness of a dense unpatterned brush monolayer synthesised under identical conditions. Both the surface shear stress measured for PCysMA brushes under water and the coefficient of friction measured in ethanol are closely correlated to the feature height, and hence to the chain conformation.

Received 3rd January 2017,
Accepted 9th February 2017

DOI: 10.1039/c7sm00013h

rsc.li/soft-matter-journal

Introduction

When polymer chains are grafted densely to a planar surface and immersed in a good solvent, steric or electrostatic repulsion may cause them to adopt an extended conformation known as a brush.[1] Polymer brushes have attracted considerable interest for various technological applications, including the control of biofouling[2–4] and lubrication.[5–8] Polymer brushes can provide highly lubricious, non-biofouling surfaces. In particular, zwitterionic poly(2-(methacryloyloxy)ethyl phosphoryl choline) (PMPC) brushes have been shown to exhibit "super-lubricious" properties.[5] However, the properties of such surface-bound chains critically depend on the brush grafting density. The brush-like properties are lost at lower grafting densities, with surface-confined chains adopting a "mushroom" (or even "pancake") conformation.

The importance of understanding the relationship between the grafting density and the resulting properties of brush layers has prompted fundamental studies of structure–property relationships. In "grafting from" methods such as atom transfer radical polymerisation (ATRP),[9,10] this may be achieved by varying the surface initiator density prior to growing the brush chains.[11] There has been much interest in brush gradients,[12] in which the grafting density varies spatially in a well-defined fashion.[13–15] This approach provides a convenient means to examine how the brush properties depend on the grafting density.[16,17]

The influence of the grafting density on brush properties is particularly acute in nanostructured polymers, which are important for technological applications but also in fundamental investigations of single-asperity contacts between molecular materials. Zauscher and co-workers demonstrated that for these systems, the chain organisation can be rather different from that observed in macroscopically extended brush layers,[18–21] with increased lateral chain mobility in very small structures (<100 nm) yielding reduced brush height compared to an unpatterned polymer formed under similar conditions.[21]

There has been significant interest in using nanotribological approaches to characterise the frictional properties of brush layers.[16,22–25] Friction force microscopy (FFM)[26,27] enables quantitative investigation of sliding interactions with nm-scale spatial

[a] *Department of Chemistry, University of Sheffield, Brook Hill, Sheffield S3 7HF, UK*
[b] *King Saud University, Riyadh, Saudi Arabia*

resolution, and has attracted widespread interest as a means to investigate not only the lubricious properties of brushes but also to investigate structure–property relationships in a broader sense, including, for example, solvent effects and ionic interactions.[6,16,22,28–31] However, a significant limitation in the use of FFM to characterise molecular materials is that, until recently, the contact mechanics describing the tip-sample interaction were poorly understood. Examination of the literature reveals a lack of agreement regarding even seemingly straightforward questions, such as whether the friction–load relationship is linear or sub-linear or how to choose the most appropriate model for interpreting friction and adhesion data. Many authors have analysed their data using macroscopic approaches such as Amontons' law, while others have used single asperity models such as the Johnson–Kendall–Roberts (JKR) or Derjaguin–Muller–Toporov (DMT) models.[26,32,33]

We have suggested that previous studies have given too little consideration to the importance of the solvent.[34] In previous studies of monolayer systems, we have shown that the contact mechanics depend on the solvation state of the molecular surface. The friction force may be treated as the sum of shearing and "molecular ploughing" components.[34–36] When the sliding surfaces are strongly solvated, shear contributions to friction are negligible and the friction–load relationship is linear. However, for media in which the surface is less well solvated, shearing becomes important, and a sub-linear friction–load relationship is observed. Recently we investigated the frictional properties of PMPC brushes using this approach.[37] The change in contact mechanics with solvent was rationalised in terms of the differences in polymer–solvent interactions, but the range of observed behaviour was nevertheless rather broad and a more detailed understanding of how brush properties are related to FFM measurements is required.

Photochemistry provides a convenient means to modify brush density at surfaces.[38–40] ATRP initiator-functionalised planar surfaces can be conveniently modified by C–Br bond photolysis.[38] Here we control UV exposure times to produce surfaces with systematically varying initiator densities, and use these model substrates to grow brushes over a range of grafting densities. We also utilise interferometric lithography (IL) to conduct nm-scale patterning. In IL, two coherent laser beams interact to produce an interferogram consisting of alternating bands of constructive and destructive interference; by carefully controlling the exposure conditions, surface features can be produced with varying dimensions. Varying the period in the interferogram provides control over the grafting density and hence produces brushes of systematically varying height. Studies of such systems by FFM provide insights into tip-sample contact mechanics, the role of the solvent in controlling brush structure and properties, and the effect of grafting density on brush height and mechanical properties.

Experimental

Materials

Silicon wafers ((100) orientation, boron-doped, test grade, 380 nm thick) were supplied by Compart Technology (Peterborough, UK). Electron microscope grids (2000 mesh Cu) used for micron-scale patterning were purchased from Agar (Cambridge, UK). 3-Aminopropyl triethoxysilane (APTES) (≥99%), triethylamine (≥99%), α-bromoisobutyryl bromide (BIBB) (98%), copper(I) bromide (≥99%), copper(II) bromide (99.9999%), 2,2′-bipyridyl (>99%), dimethylphenyl phosphine (DMPP) (99%), L-cysteine (98%), 3-(acryloyloxy)-2-hydroxypropyl, and 11-mercapto-undecanoic acid (MUA) were obtained from Sigma-Aldrich (Gillingham, UK). Sulfuric acid (≥95%), hydrogen peroxide (30% v/v), ethanol (HPLC grade), toluene (HPLC grade), dichloromethane (HPLC grade), ammonia solution (s.g. 35%), and methanol (HPLC grade) were supplied by Fisher Scientific (Loughborough, UK). Dry toluene was collected from an in-house Grubbs dry solvent system. Deionised water was obtained from an Elga PURELAB apparatus with a resistivity of 15 MΩ cm.

Glassware and silicon wafers in glass tubes were thoroughly cleaned by sonication in a 50 : 50 ethanol/acetone mixture for 30 min, followed by sonication in water for 30 min. The substrates were immersed in piranha solution, consisting of sulfuric acid (70%) and hydrogen peroxide (30%), for 40 min (**Warning!** Piranha solution is an extremely strong oxidising agent that has been known detonate spontaneously upon contact with organic materials), and rinsed more than seven times in deionised water. They were then subjected to a further cleaning cycle using the RCA (Radio Corporation of America) solution (70% deionised water, 15% hydrogen peroxide, and 15% ammonia) which was boiled for 40 min. The substrate was rinsed seven times with deionised water and sonicated in water for 15 min, and placed in a 120 °C oven overnight to dry.

Amine-functionalised films were made by immersing dry silicon wafers in a 0.2 M APTES solution in dry toluene under nitrogen for 30 min, with sonication during the first 5 min. The coated wafers were rinsed in toluene and ethanol and then blown dry with nitrogen. Subsequently, wafer surfaces were annealed by placing them in a 120 °C vacuum oven for 40 min. Prior to performing atom transfer radical polymerization, ATRP initiator sites were introduced by immersing the aminosilane films in a solution of 2-bromoisobutyryl bromide (0.37 mL, 3 mmol) and triethylamine (0.41 mL, 4 mmol) in dichloromethane (DCM; 60 mL) for 40 min. Finally, the treated substrates were sonicated in dichloromethane and ethanol for 5 min and then dried under nitrogen.

Synthesis of cysteine methacrylate monomer (CysMA)

CysMA was synthesised according to the method reported by Alswieleh *et al.*[41] L-Cysteine (15.13 g, 124.88 mmol) was dissolved in 100 mL deionised water, and transferred to a 250 mL round-bottomed flask. 3-Acryloxy-2-hydroxy methacrylate (29.43 g, 137.36 mmol) was added slowly into the stirred aqueous solution, followed by dimethylphenyl phosphine (20 μL, 147 μmol) as a catalyst. The mixture was stirred for 2 h at room temperature. The product was washed twice with ethyl acetate (50 mL) and dichloromethane (2 × 50 mL).

The flask was connected to a rotary evaporator operating under reduced pressure to remove excess solvent. The concentrated aqueous solution (CysMA monomer) was isolated and

crystallised in the freezer before drying overnight. The final white solid powder (39.6 g, 94% yield) was stored under nitrogen in the fridge.

Surface photopatterning of ATRP initiator sites

Surface photopatterning of BIBB-functionalised substrates was conducted using a 100 mW Coherent Innova 300 C FreD frequency-doubled argon ion laser (Coherent UK, Ely, UK) operating at 244 nm. Micrometre-scale patterns were obtained by irradiating substrates through a copper electron microscope grid (2000 mesh, Agar, Cambridge, UK). The diameter of the illuminated area was 0.5 cm^2. Interferometric lithography (IL) was used to fabricate nm-scale patterned substrates using a Lloyd's mirror two-beam interferometer, as described previously.[41–43] The angle 2θ between the two laser beams was controlled using a rotating stage, enabling the period of the resulting patterns to be controlled. The interferogram consists of alternating bands of constructive and destructive interference, with a sinusoidal cross-section such that the period is given by $\lambda/\sin 2\theta$.

Polymerisation reactions

Patterned and unpatterned substrates were loaded into carousel tubes, which were purged three times with nitrogen and then filled with dry nitrogen. CysMA monomer (5.0 g, 15.0 mmol) was placed in a round-bottom flask and deionised water (12 mL) was added. The solution was degassed under nitrogen for 30 min. Copper(I) bromide (71.4 mg, 0.5 mmol), copper(II) bromide (55.6 mg, 0.25 mmol), and 2-2′-bipyridyl (234 mg, 1.50 mmol) were added. After mixing and degassing for 10 min, the mixture was sonicated for 2–3 min. To commence the surface ATRP of CysMA, 5–7 mL of the monomer–catalyst solution was subsequently transferred to the carousel tube to cover the sample, the carousel was shaken well and left for 1.5 h at 21 °C. After a pre-determined polymerisation time, brush-coated substrates were sonicated in water, rinsed using water and ethanol respectively, and dried using a nitrogen sparge.

Modification of the AFM probes

Commercial V-shaped silicon nitride (Si_3N_4) probes (model NP, with a nominal normal force constant 0.06 N m^{-1}) were cleaned by immersion in cold piranha solution for 15–20 min. They were then carefully rinsed seven times by immersion in deionised water, flooded with water from a wash bottle and finally rinsed in HPLC-grade ethanol before being dried under a very slow stream of nitrogen. The treated probes were left overnight to dry at room temperature prior to gold deposition. They were coated with 1–2 nm chromium (Cr chips, 99.99% purity, Agar, Scientific) at a deposition rate of 0.01 nm s^{-1} followed by 10 nm gold (Au wire, 99.99%, Advent Research Materials Ltd) using a deposition rate of 0.02 nm s^{-1} in an Edwards Auto 306 bell jar vacuum coater system. Subsequently, the coated probes were immersed in a 1.0 mM solution of 11-mercaptoundecanoic acid (MUA) in degassed HPLC-grade ethanol for approximately 24 h. The acid-functionalised cantilevers were immersed in ethanol through the entire period of the experiments to protect the thiol monolayer from ambient oxidation.

Friction force microscopy (FFM)

FFM measurements were conducted using a Digital Nanoscope Vlll multi-mode Atomic force microscopy (Multimode Vlll, Bruker, UK) operating in contact mode, using E-scanner using probes functionalised with 11-mercaptoundecanoic acid. A liquid cell (MTFML-V2, Bruker, UK) fitted with a plastic O-ring (Bruker, UK) were used to perform friction measurements in different media. Friction forces were acquired from friction loops obtained from forward–reverse scanning of single lines. The measurements were performed at a scan rate of 1.4 Hz with 256 samples per line and a 90° scan angle. The normal applied load was reduced stepwise in increments of 0.2 V, being reduced from 2.0 V until the tip separated from the sample surface. Four to six locations were examined on each sample, and at least two samples were used for each data point, using two different cantilevers in each experiment. Normal calibration of the cantilevers was carried out by first determining the deflection sensitivity (nm V^{-1}) of the probes from the slope of the repulsive part of a force curve acquired on the flat surface of mica. Second, the spring constant of the cantilever was calculated from the power spectral density of its thermal spectra at room temperature, using multi-mode Vlll AFM, following the method introduced by Hutter and Bechhofer.[44]

The lateral stiffness was determined using the wedge calibration method introduced by Olgetree *et al.*[45] and refined by Varenberg *et al.*[46] More specifically, the cantilever was scanned across a commercially available silicon grating TGF11 (MikroMasch, Tallinn, Estonia) and the friction signal was obtained as a function of the applied load. The lateral force was calibrated in each solution used for the measurements. The tip radius was measured by imaging a calibration grating TGG01 (MikroMasch, Tallinn, Estonia) at scanning angles of 0° and 90°, respectively. The profile of the tip was determined following the Zenhausen model of deconvolution.[47] To minimise tip losses and avoid contamination, all calibrations were performed immediately after each experiment using the same solution in which the friction measurements had been performed.

Results and discussion

Polymer brush growth

APTES films were brominated by amidation using excess BIBB, and PCysMA brushes were grown from these initiator-functionalised surfaces *via* ATRP. The dry brush thicknesses were determined using ellipsometry. Fig. 1 shows the variation in ellipsometric brush thickness with polymerisation time. There is an approximately linear relationship between the mean brush thickness and polymerisation time for the first 90 min. Thereafter, the brush thickness increases more slowly over time. A fixed polymerisation time of 90 min was selected for the remainder of the work described here, giving a brush thickness of 7 nm. Up to this thickness the brush growth was

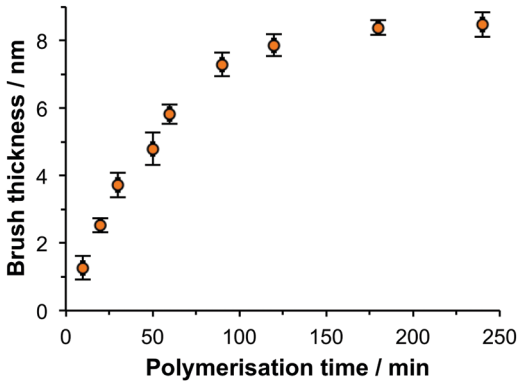

Fig. 1 Variation in dry brush thickness with polymerisation time for PCysMA brushes as determined using ellipsometry. Micropatterned brushes.

uniform and rapid, and films could be prepared repeatably. Because the properties of the brushes were expected to depend strongly on the degree of polymerisation, it was important to control the polymerisation conditions carefully.

PCysMA brushes were characterised by XPS. The spectra obtained were similar to those reported previously by Alswieleh *et al.*[41] More specifically, C 1s spectra were fitted using three components with binding energies of 285.0, 286.3, and 288.7 eV, which correspond to C–C–C, C–C═O/C–C–N, and O–C═O, respectively. The C–C–C, C–C═O/C–C–N, and O–C═O atomic ratios in the fitted C 1s spectrum were 2.1 : 1.3 : 1.0, matching the calculated ratios of 2.0 : 1.3 : 1.0.

BIBB–APTES films were exposed to UV light through a mask, and PCysMA brushes were grown by surface ATRP. The dry samples were imaged by AFM and the height difference between the masked and exposed regions was measured (Fig. 2). The height difference increases rapidly at low doses, reaching a limiting value of *ca.* 7 nm after a dose of 3 J cm^{-2}. UV-induced photolysis of the C–Br bond leads to removal of the initiator groups in exposed areas, leading to a corresponding reduction in brush density during ATRP and hence a reduction in the apparent brush thickness. A limiting height difference is reached when all the Br has been removed in the exposed regions and no PCysMA chains can grow. The height difference under these conditions is equal to the thickness of the continuous dense brush layer that is formed in the masked regions. The data in Fig. 2 indicate that a dose of 3 J cm^{-2} is required in order to ensure complete removal of Br from the surface. The height difference between the masked and exposed regions is ~7 nm, which is comparable to the ellipsometric thickness of a continuous, unpatterned brush film formed under the same polymerisation conditions.

Friction force microscopy studies of PCysMA brushes

Fig. 3 shows friction–load plots obtained for the PCysMA brushes immersed in two liquids. Water is a good solvent for PCysMA and binds strongly, causing swelling of the brush layers. In contrast, ethanol is a poor solvent for PCysMA. Clearly, the friction–load relationship is linear in the latter solvent but sub-linear in the former. Moreover, for a given load,

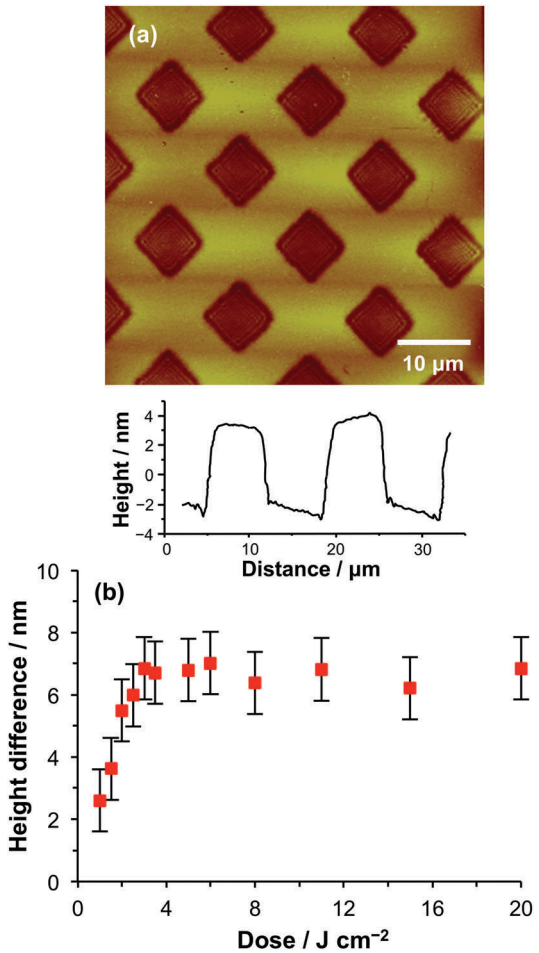

Fig. 2 (a) AFM height image of a dry micropatterned PCysMA brush layer obtained after UV exposure (λ = 244 nm) of a brominated initiator surface through a mask followed by ATRP, together with a representative line section. A dry, unpatterned brush prepared under identical conditions had a thickness of 7 nm. (b) Variation in brush height difference between masked and exposed regions of micropatterned brushes as a function of UV dose during patterning.

the friction force is larger in water than in ethanol. The friction–load plots in water were modelled and fitted using the DMT model for contact mechanics.

In an earlier study of PMPC brushes, linear friction–load plots were attributed to two different conformations: highly swollen brushes in methanol (which is a good solvent for PMPC) for which adhesion was negligible, and collapsed brushes (obtained in 2-propanol, which is a poor solvent for PMPC).[37] In both cases, energy dissipation occurs *via* "molecular ploughing" *i.e.* by deformation of polymer chains as the tip slides across the film. For poorer solvents than methanol, different behaviour was observed. For surface-grafted PMPC brushes immersed in either water or ethanol, non-linear friction–load relationships were observed. For these two solvents, the thermodynamic work of adhesion is relatively small because the PMPC chains are highly solvated. However, these brushes have low elastic moduli and hence the tip-sample contact area is large. When multiple weak brush interactions

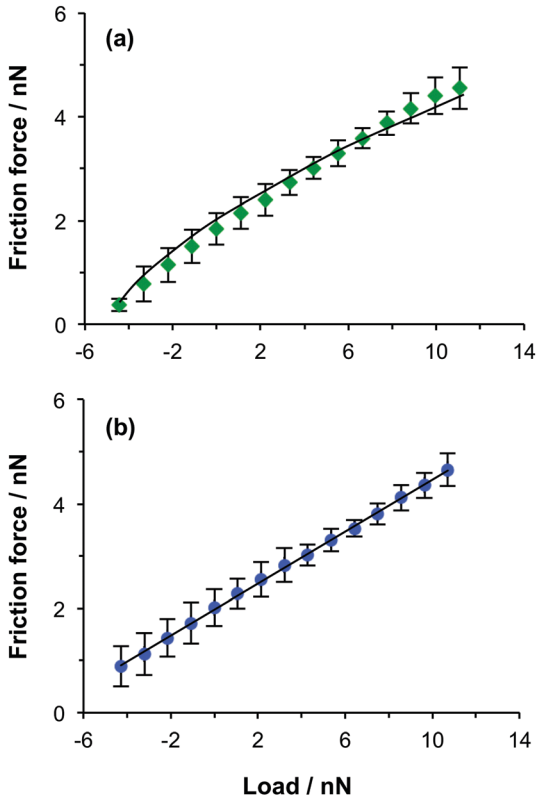

Fig. 3 Friction–load plots obtained for PCysMA brushes with a dry thickness of 7 nm immersed in (a) water and (b) ethanol. Data acquired in the former solvent have been fitted using the DMT model, while a straight line has been fitted by linear regression for the data set acquired in the latter solvent.

are integrated across a large contact area, a significant adhesive interaction results.

We hypothesise that a similar explanation holds for the data shown in Fig. 3. The friction force F_F may be regarded as the sum of load-dependent (ploughing) and area-dependent (shearing) terms.[26,48] The situation may be summarised quantitatively as follows:[35–37]

$$F_F = \mu(F_N + F_a) + \pi\left(\frac{R}{K}\right)^{\frac{2}{3}}\tau(F_N + F_a)^{\frac{2}{3}} \quad (1)$$

where F_N is the load, F_a is the pull-off force, R is the tip radius, K is the elastic modulus and τ is the surface shear strength. In ethanol, the solvent–polymer interaction is relatively weak, and the brush is less swollen; ploughing dominates, and the second term in eqn (1) is negligible, leading to a linear friction–load relationship. In water, the brushes are highly solvated and swollen. However, the contact area is large, despite the small work of adhesion, so that the second term in eqn (1) makes a significant contribution to energy dissipation, leading to a non-linear friction–load relationship.

Tribological properties of brushes with varying grafting densities

Bromine-functionalised APTES films were exposed to UV light for various time periods to yield a range of surface initiator densities. No mask was used in these experiments, so the initiator density was uniform across the entire surface. PCysMA chains were grown from these surfaces *via* ATRP to produce a library of brushes of varying density. The friction force was then measured for each sample as a function of applied load in both ethanol and water.

In ethanol, the friction–load relationship was always linear regardless of the UV exposure time (Fig. 4a). In this solvent, even the most densely-grafted polymer chains did not form fully swollen brushes. The sliding interaction is dominated by dissipation of energy in molecular ploughing *via* conformational changes in the polymer chains.

In water, the friction–load relationship was found to be non-linear for UV doses less than 1.5 J cm^{-2} (Fig. 4b). However, a linear friction–load relationship was obtained for higher UV doses. According to Fig. 2, the height difference between the masked and exposed regions of a micropatterned substrate is *ca.* 4 nm after a UV dose of 1.5 J cm^{-2}, indicating that slightly more than 50% of the polymer brush layer has been removed. The transition to linear friction–load behaviour under these conditions is probably the result of this reduction in surface chain density, which causes PCysMA chains to adopt a collapsed "mushroom" conformation.

The friction–load data were fitted using eqn (1). The surface shear strength τ was determined, and is shown as a function of the UV dose in Fig. 4c. Initially, the value of τ increases with UV dose, reaching a maximum value at approximately 0.5 J cm^{-2}. This suggests that, at low UV doses, more energy is dissipated *via* shearing as the polymer brush density is reduced. Although counter-intuitive, this observation can be rationalised using the same explanation invoked for the non-linear friction–load relationship in Fig. 3a: for lower brush densities, the effective modulus of the polymer brush layer is reduced, and the contact area increases further. The brushes are highly solvated in water, so the thermodynamic work of adhesion remains small. However, it is not zero and the increase in the contact area causes a net increase in the adhesive energy leading to more effective energy dissipation *via* shearing.

Eventually, however, the density of the polymer layer is reduced to such an extent that the grafted chains begin to adopt a collapsed conformation. As this transition occurs, the contribution of ploughing to energy dissipation becomes more important. A limiting value of τ is reached, and this remains unchanged as the UV exposure increases above 1.5 J cm^{-2}. At these higher UV doses, ploughing is expected to be the dominant pathway for energy dissipation. For UV doses greater than 1.5 J cm^{-2}, we infer that the PCysMA chains predominantly adopt a collapsed conformation. This conclusion is consistent with the qualitative interpretation of the linear friction–load plots in this UV dose regime, suggesting that energy dissipation is dominated by ploughing.

Nanopatterned brushes

Nanostructured materials were prepared using interferometric lithography. In IL, two coherent beams of light interfere to produce an interferogram comprising alternating bands of

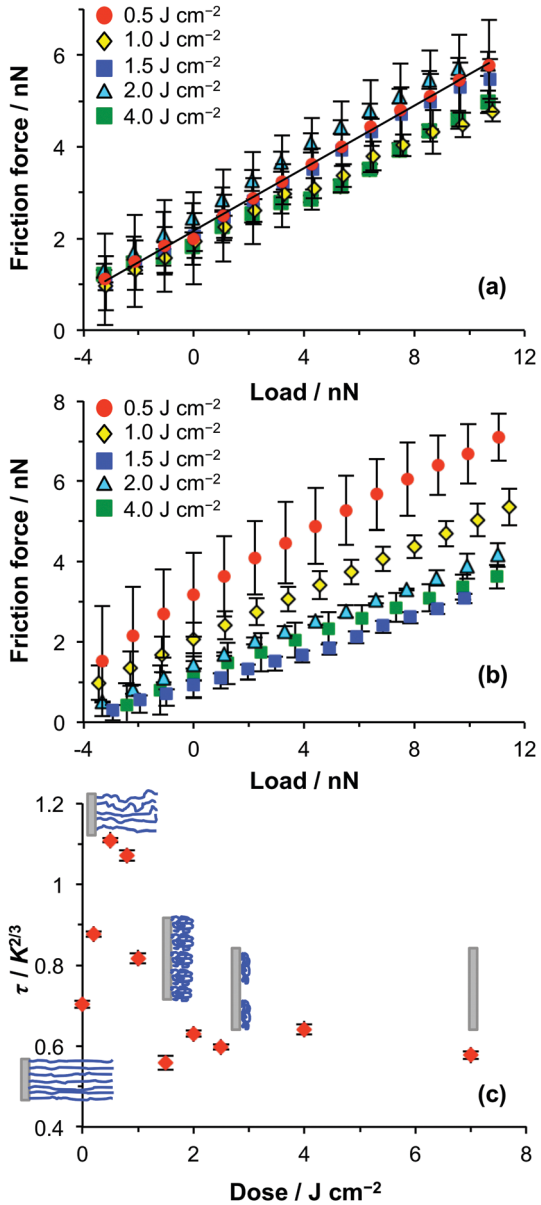

Fig. 4 (a) Friction–load plots acquired in ethanol for a series of PCysMA brushes grown from bromine-functionalised planar surfaces subjected to varying UV doses. The data were fitted using linear regression and linear friction–load relationships were observed in all cases. For clarity, only one fit is shown for a UV dose of 0.5 J cm^{-2}. (b) Friction–load plots acquired in water for a series of PCysMA brushes grown from bromine-functionalised surfaces subjected to varying UV doses. Fits are shown for UV doses of 0.5 J cm^{-2} (DMT) and 2.0 J cm^{-2} (linear). (c) Variation in the surface shear strength determined in water as a function of the UV dose. Schematic diagrams illustrate the change in polymer conformation with grafting density.

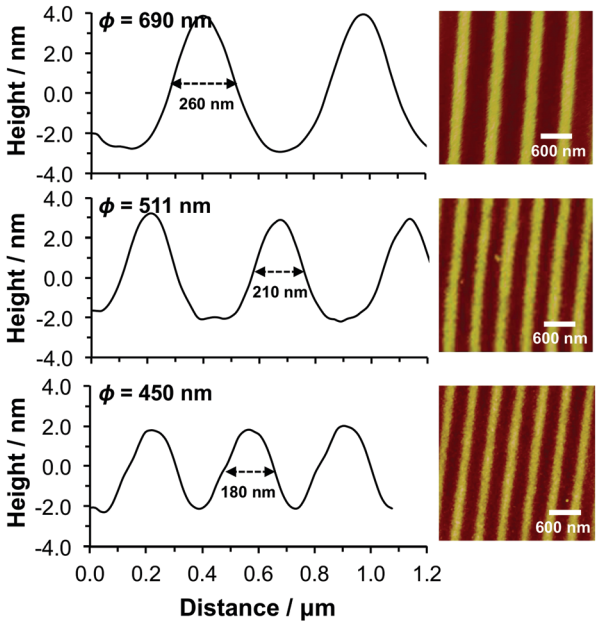

Fig. 5 Left: Mean AFM height sections through topographical images (right) acquired for nanostructured PCysMA brushes formed with periods ϕ in the range 450–690 nm.

constructive and destructive interference with a sinusoidal cross-section. Exposing an ATRP initiator-functionalised surface to such an interferogram leads to dehalogenation. In regions exposed to intensity maxima, there is extensive modification of the surface, while in regions exposed to minima, there is negligible surface modification. Between these maxima and minima there is a gradient in Br density. Patterned Br-functionalised surfaces formed by IL were used to prepare nanopatterned PCysMA brushes *via* ATRP. Fig. 5 shows height sections through three different specimens (determined for a dry brush layer). The UV dose was 1.8 J cm^{-2} in all three cases. However, the angle between the mirror and substrate was adjusted in each case in order to vary the period.

For a surface pattern formed with a period of 690 ± 15 nm, the full width at half maximum height (FWHM) was 260 nm, and the height difference between the highest and lowest points in the brush cross-section was ~7 nm. This indicates that, at this UV dose, the PCysMA chains grown from the regions exposed to minima in the interferogram swell to a similar extent as fully dense non-patterned PCysMA brushes, or brushes in the masked regions when UV exposure was conducted using a grid consisting of micrometre-scale features (Fig. 2).

However, the height difference between the highest and lowest points in the patterns decreased as the period was gradually reduced, reaching *ca.* 5 nm at a period of 511 ± 15 nm (FWHM 205 nm) and *ca.* 4 nm at a period of 450 ± 10 nm (FWHM 175 nm). A change in period is not expected to produce any change in the UV intensity at the maxima and minima of the interferogram. However, smaller periods lead to a reduction in the mean width of the polymer nanostructure.

Previous work by Zauscher and co-workers provides an explanation for these observations. For nanostructured poly(*N*-isopropylacrylamide-*co*-methacrylic acid) copolymer brushes produced *via* electron beam lithography, the mean brush height increased with increasing feature size, which was attributed to a concomitant reduction in lateral chain mobility.[20] For the periodic structures reported in the present study, we hypothesise that increasing the feature width also leads to a reduction in the lateral chain mobility. Brushes extend away from the substrate because of mutual repulsive interactions

between neighbouring chains. However, such chain–chain repulsion is reduced for lower grafting densities or, as in the present case, where the lateral dimensions of the nanostructured brush become sufficiently small. For structures with a FWHM of 260 nm, the grafting density in the highest parts of the nanostructures is presumably similar to that of an unpatterned brush, leading to a similar degree of chain extension from the surface. However, as the period becomes smaller, the greater lateral mobility of the chains within the centre of the nanostructure leads to less swelling and a gradual reduction is observed in the mean feature height.

The frictional properties of the patterned brushes were determined in both water and in ethanol. To enable quantification of the data obtained for such complex samples, the difference in friction ΔF_F between the maxima and minima in line sections through friction images was measured. Plots of ΔF_F against load were acquired in both liquids. A non-linear friction–load relationship was observed for all patterned brushes immersed in water, and such data could be satisfactorily fitted using DMT mechanics (Fig. 6a). The surface shear stress was determined and is shown in Fig. 6b as a function of the FWHM of the nanostructures. The minimum value of τ was obtained for samples with a FWHM of 137 nm. The surface shear strength increased for larger periods. For samples with a width of 260 nm, the surface shear stress approached that obtained for a micrometre-scale pattern, which effectively represents the limit of a fully-formed, continuous PCysMA brush. It is notable that the surface shear stress for the sample with a width (FWHM) of 260 nm was approximately three times larger than that determined for the sample with a width of 137 nm. This suggests that this apparently modest change in the lateral dimensions of these polymer nanostructures produces a substantial change in the chain mobility.

The greater surface shear stress closely correlated with the increase in nanostructured brush height. This is consistent with the explanation given above for the change in brush height: as the period in the patterned sample increases, there is a concomitant increase in the width of the region close to the minimum in the interferogram that retains a sufficiently high Br density to support the formation of a densely-grafted brush layer. Eventually, as the feature width approaches 300 nm, the grafting density in this central region becomes high enough to cause the PCysMA chains to swell significantly, so the heights of the nanostructures approach the thickness of the brushes formed on the micropatterned sample. The heights of these nanostructures changed significantly as the width increased

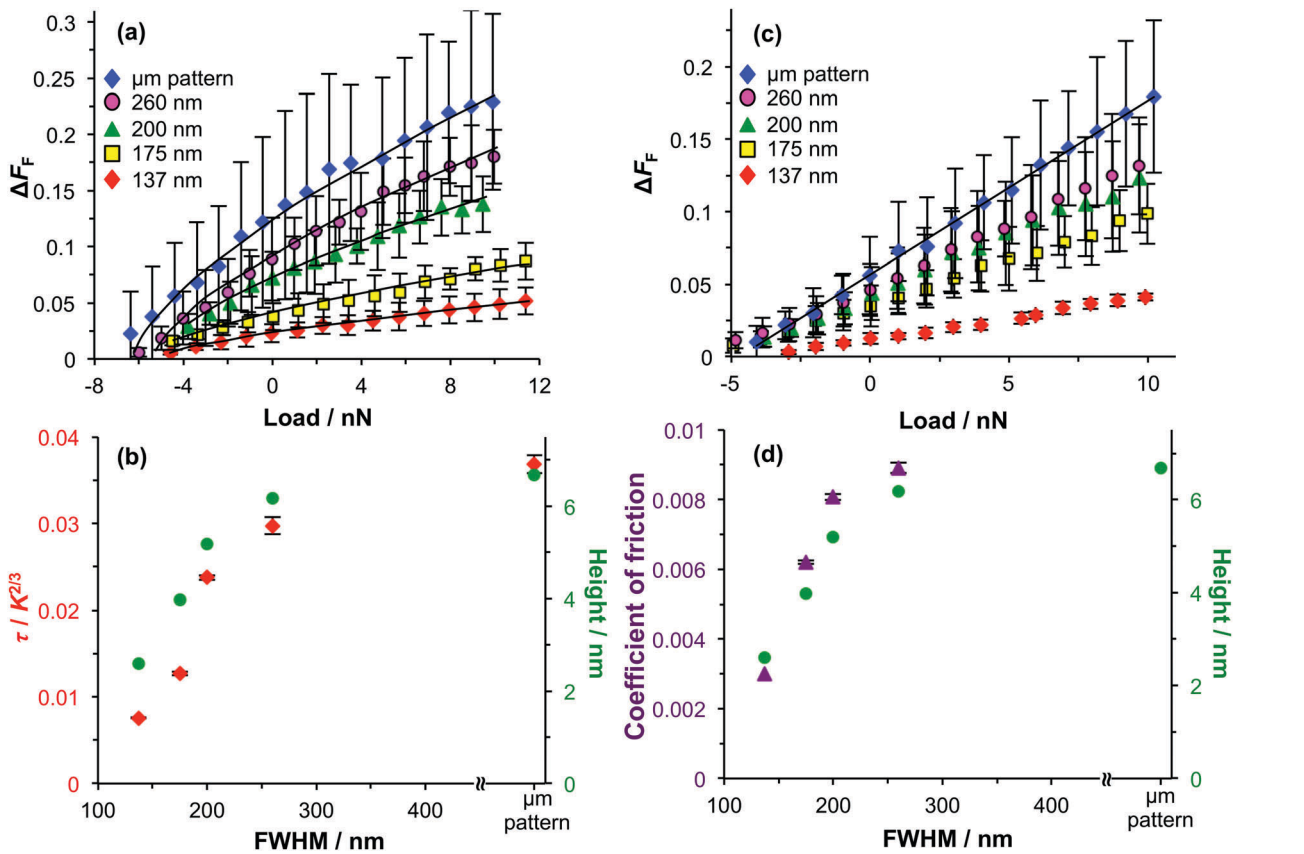

Fig. 6 (a) Variation in the peak-trough friction difference with load for brushes of varying (dry) feature size after immersion in water. Data fits (black lines) were obtained assuming DMT mechanics. (b) Variation in the surface shear strength with feature size for brushes immersed in water (diamonds). (c) Variation in the peak-trough friction difference with load for brushes of varying feature size immersed in ethanol. (d) Variation in the coefficient of friction with dry feature size for brushes immersed in ethanol (triangles). (c and d) Also show the variation in heights of the dry polymer structures as a function of dry feature size.

from 137 to 260 nm, which is consistent with the hypothesis that a substantial change occurred in the lateral chain mobility across this range of feature size.

Friction–load plots were also acquired in ethanol (Fig. 6c). A linear friction–load relationship was observed for all samples, which is consistent with the hypothesis that the grafted chains adopt a ''mushroom'' morphology in this solvent such that energy dissipation is dominated by ploughing and shear contributions are negligible. The variation in the coefficient of friction with the period of the brush nanostructures correlated closely with the variation in the feature height (Fig. 6d), indicating that the chain grafting density in the regions of the surface exposed to minima in the interferogram also has a pronounced influence on the rate of energy dissipation in ploughing.

These data suggest that measurements of brush height for patterned substrates provide a valuable approach to predict the variation in physical properties that depend on the grafting density. While the grafting density is difficult to measure directly, brush height measurements are comparatively straightforward and Fig. 6 indicates that the latter parameter directly affects both the surface shear strength and the coefficient of friction. In the former case, a greater brush density leads to a change in the tip contact area and hence to stronger adhesion between the probe and the polymer chains. This enables enhanced energy dissipation through molecular ploughing and hence a higher coefficient of friction.

The data obtained for nanostructured grafted polymers indicate that for surface coatings designed to modify friction, the morphology of the surface film is very important. In particular, below a critical size, grafted polymers may exhibit significant changes in their tribological characteristics relative to those of continuous films formed from polymers of similar molecular weight.

Conclusions

Photochemical methods provide a simple but versatile route to a library of planar surfaces with systematically varying ATRP initiator densities. This can be achieved by either producing spatially uniform monolayers, or by using interferometric lithography to generate nm-scale patterns. UV photolysis of C–Br bonds at 244 nm leads to dehalogenation of bromine-functional initiator sites. These surfaces can be used to grow zwitterionic polymer brushes of tunable grafting density by ATRP. PCysMA chains are strongly solvated when immersed in water, leading to a relatively small thermodynamic work of adhesion, but the weak elastic modulus of such brush layers leads to a large contact area with an AFM probe. This causes significant shearing, leading to a sublinear friction–load relationship that is well-fitted by DMT mechanics. Initially, the surface shear stress increases as the grafting density is reduced, but then decreases to reach a limiting value at a brush grafting density of approximately 50% of that of an unmodified surface. At this density, the friction–load relationship becomes linear and is dominated by molecular ploughing. In contrast, in ethanol, which is a poor solvent for PCysMA, a linear friction–load relationship is observed under all conditions because energy dissipation is dominated by ploughing. When nanoscale-patterned surface structures are prepared using interferometric lithography, the height difference between regions exposed to maxima and minima in the interferogram approaches the thickness of a continuous dense brush at feature widths of $\sim$300 nm. The shear stress (determined in water) and the coefficient of friction (measured in ethanol) both increase in proportion to the increase in brush height difference between these two regions.

Acknowledgements

The authors thank EPSRC (Programme Grant EP/I012060/1) for Financial Support.

Notes and references

1 F. Brochard-Wyart, P. G. de Gennes, L. Leger, Y. Marciano and E. Raphael, Adhesion promoters, *J. Phys. Chem.*, 1994, **98**, 9405–9410.
2 H. Ma, D. Li, X. Sheng, B. Zhao and A. Chilkoti, Protein resistant polymer brushes on silicon oxide by surface initiated atom transfer radical polymerization, *Langmuir*, 2006, **22**, 3751–3756.
3 H. Ma, M. Wells, T. P. Beebe, Jr. and A. Chilkoti, Surface initiated polymerization of nonfouling polymer brushes of oligoethylene glycol methacrylate on gold, *Adv. Funct. Mater.*, 2006, **16**, 640–648.
4 A. Hucknall, S. Rangarajan and A. Chilkoti, In Pursuit of Zero: Polymer Brushes that Resist the Adsorption of Proteins, *Adv. Mater.*, 2009, **21**, 2441–2446.
5 M. Chen, W. H. Briscoe, S. P. Armes and J. Klein, Lubrication at Physiological Pressures by Polyzwitterionic Brushes, *Science*, 2009, **323**, 1698–1701.
6 R. M. Espinosa-Marzal, R. M. Bielecki and N. D. Spencer, Understanding the role of viscous solvent confinement in the tribological behavior of polymer brushes: a bioinspired approach, *Soft Matter*, 2013, **9**, 10572–10585.
7 M. Kobayashi and A. Takahara, Tribological properties of hydrophilic polymer brushes under wet conditions, *Chem. Rec.*, 2010, **10**, 208–216.
8 M. Müller, S. Lee, H. A. Spikes and N. D. Spencer, The Influence of Molecular Architecture on the Macroscopic Lubrication Properties of the Brush-Like Co-polyelectrolyte Poly(L-lysine)-g-poly(ethylene glycol) (PLL-g-PEG) Adsorbed on Oxide Surfaces, *Tribol. Lett.*, 2003, **15**, 395–405.
9 T. E. Patten and K. Matyjaszewski, Atom Transfer Radical Polymerization and the Synthesis of Polymeric Materials, *Adv. Mater.*, 1998, **10**, 901–915.
10 K. Matyjaszewski and J. Xia, Atom Transfer Radical Polymerization, *Chem. Rev.*, 2001, **101**, 2921–2990.
11 Z. Bao, M. L. Bruening and G. L. Baker, Control of the Density of Polymer Brushes Prepared by Surface-Initiated

Atom Transfer Radical Polymerization, *Macromolecules*, 2006, **39**, 5251–5258.
12 S. Morgenthaler, C. Zink and N. D. Spencer, Surface-chemical and -morphological gradients, *Soft Matter*, 2008, **4**, 419–434.
13 T. Wu, K. Efimenko and J. Genzer, Combinatorial Study of the Mushroom-to-Brush Crossover in Surface Anchored Polyacrylamide, *J. Am. Chem. Soc.*, 2002, **124**, 9394–9395.
14 P. Gong, T. Wu, J. Genzer and I. Szleifer, Behavior of Surface-Anchored Poly(acrylic acid) Brushes with Grafting Density Gradients on Solid Substrates: 2. Theory, *Macromolecules*, 2007, **40**, 8765–8773.
15 R. R. Patil, S. Turgman-Cohen, J. Šrogl, D. Kiserow and J. Genzer, On-Demand Degrafting and the Study of Molecular Weight and Grafting Density of Poly(methyl methacrylate) Brushes on Flat Silica Substrates, *Langmuir*, 2015, **31**, 2372–2381.
16 S. N. Ramakrishna, R. M. Espinosa-Marzal, V. V. Naik, P. C. Nalam and N. D. Spencer, Adhesion and Friction Properties of Polymer Brushes on Rough Surfaces: A Gradient Approach, *Langmuir*, 2013, **29**, 15251–15259.
17 I. Lilge and H. Schönherr, Control of Cell Attachment and Spreading on Poly(acrylamide) Brushes with Varied Grafting Density, *Langmuir*, 2016, **32**, 838–847.
18 M. Kaholek, W.-K. Lee, S.-J. Ahn, H. Ma, K. C. Caster, B. LaMattina and S. Zauscher, Stimulus-Responsive Poly-(N-isopropylacrylamide) Brushes and Nanopatterns Prepared by Surface-Initiated Polymerization, *Chem. Mater.*, 2004, **16**, 3688–3696.
19 M. Kaholek, W.-K. Lee, B. LaMattina, K. C. Caster and S. Zauscher, Fabrication of Stimulus-Responsive Nanopatterned Polymer Brushes by Scanning Probe Lithography, *Nano Lett.*, 2004, **4**, 373–376.
20 M. Kaholek, W.-K. Lee, J. Feng, B. LaMattina, D. J. Dyer and S. Zauscher, Weak Polyelectrolyte Brush Arrays Fabricated by Combining Electron-Beam Lithography with Surface-Initiated Photopolymerization, *Chem. Mater.*, 2006, **18**, 3660–3664.
21 W.-K. Lee, M. Patra, P. Linse and S. Zauscher, Scaling Behavior of Nanopatterned Polymer Brushes, *Small*, 2007, **3**, 63–66.
22 M. A. Brady, F. T. Limpoco and S. S. Perry, Solvent-Dependent Friction Force Response of Poly(ethylenimine)-graft-poly(ethylene glycol) Brushes Investigated by Atomic Force Microscopy, *Langmuir*, 2009, **25**, 7443–7449.
23 N. Nordgren and M. W. Rutland, Tunable Nanolubrication between Dual-Responsive Polyionic Grafts, *Nano Lett.*, 2009, **9**, 2984–2990.
24 A. Li, S. N. Ramakrishna, E. S. Kooij, R. M. Espinosa-Marzal and N. D. Spencer, Poly(acrylamide) films at the solvent-induced glass transition: adhesion, tribology, and the influence of crosslinking, *Soft Matter*, 2012, **8**, 9092–9100.
25 L. Han, J. Yin, L. Wang, K.-K. Chia, R. E. Cohen, M. F. Rubner, C. Ortiz and M. C. Boyce, Tunable stimulus-responsive friction mechanisms of polyelectrolyte films and tube forests, *Soft Matter*, 2012, **8**, 8642–8650.
26 R. W. Carpick and M. Salmeron, Scratching the Surface: Fundamental Investigations of Tribology with Atomic Force Microscopy, *Chem. Rev.*, 1997, **97**, 1163–1194.
27 E. Gnecco, R. Bennewitz, T. Gyalog and E. Meyer, Friction experiments on the nanometre scale, *J. Phys.: Condens. Matter*, 2001, **13**, R619–R642.
28 F. T. Limpoco, R. C. Advincula and S. S. Perry, Solvent Dependent Friction Force Response of Polystyrene Brushes Prepared by Surface Initiated Polymerization, *Langmuir*, 2007, **23**, 12196–12201.
29 X. Liu, E. Thormann, A. Dedinaite, M. Rutland, C. Visnevskij, R. Makuska and P. M. Claesson, Low friction and high load bearing capacity layers formed by cationic-block-non-ionic bottle-brush copolymers in aqueous media, *Soft Matter*, 2013, **9**, 5361–5371.
30 Z. Zhang, A. J. Morse, S. P. Armes, A. L. Lewis, M. Geoghegan and G. J. Leggett, Effect of Brush Thickness and Solvent Composition on the Friction Force Response of Poly(2-(methacryloyloxy)ethylphosphorylcholine) Brushes, *Langmuir*, 2011, **27**, 2514–2521.
31 Z. Zhang, M. Moxey, A. Alswieleh, A. J. Morse, A. L. Lewis, M. Geoghegan and G. J. Leggett, Effect of Salt on Phosphorylcholine-based Zwitterionic Polymer Brushes, *Langmuir*, 2016, **32**, 5048–5057.
32 J. N. Israelachvilli, *Intermolecular and Surface Forces*. Academic Press, London, 2nd edn, 1992.
33 C. M. Mate, *Tribology on the small scale*. Oxford University Press, Oxford, 2008.
34 K. Busuttil, M. Geoghegan, C. A. Hunter and G. J. Leggett, Contact Mechanics of Nanometer-Scale Molecular Contacts: Correlation between Adhesion, Friction, and Hydrogen Bond Thermodynamics, *J. Am. Chem. Soc.*, 2011, **133**, 8625–8632.
35 K. Busuttil, N. Nikogeorgos, Z. Zhang, M. Geoghegan, C. A. Hunter and G. J. Leggett, The mechanics of nanometre-scale molecular contacts, *Faraday Discuss.*, 2012, **156**, 325–341.
36 N. Nikogeorgos, C. A. Hunter and G. J. Leggett, Relationship Between Molecular Contact Thermodynamics and Surface Contact Mechanics, *Langmuir*, 2012, **28**, 17709–17717.
37 Z. Zhang, A. J. Morse, S. P. Armes, A. L. Lewis, M. Geoghegan and G. J. Leggett, Nano-Scale Contact Mechanics of Biocompatible Polyzwitterionic Brushes, *Langmuir*, 2013, **29**, 10684–10692.
38 S. A. Alang Ahmad, G. J. Leggett, A. Hucknall and A. Chilkoti, Micro- and Nanostructured Poly[oligo(ethylene glycol)methacrylate] Brushes Grown From Photopatterned Halogen Initiators by Atom Transfer Radical Polymerization, *Biointerphases*, 2011, **6**, 8–15.
39 C. Kang, R. M. Crockett and N. D. Spencer, Molecular-Weight Determination of Polymer Brushes Generated by SI-ATRP on Flat Surfaces, *Macromolecules*, 2014, **47**, 269–275.
40 C. Kang, S. N. Ramakrishna, A. Nelson, C. V. M. Cremmel, H. vom Stein, N. D. Spencer, L. Isa and E. M. Benetti, Ultrathin, freestanding, stimuli-responsive, porous membranes from polymer hydrogel-brushes, *Nanoscale*, 2015, **7**, 13017–13025.
41 A. M. Alswieleh, N. Cheng, I. Canton, B. Ustbas, X. Xue, V. Ladmiral, S. Xia, R. E. Ducker, O. El Zubir, M. L. Cartron, C. N. Hunter, G. J. Leggett and S. P. Armes, Zwitterionic

Poly(amino acid methacrylate) Brushes, *J. Am. Chem. Soc.*, 2014, **136**, 9404–9413.

42 G. Tizazu, O. El-Zubir, S. R. J. Brueck, D. G. Lidzey, G. J. Leggett and G. P. Lopez, Large area nanopatterning of alkylphosphonate self-assembled monolayers on titanium oxide surfaces by interferometric lithography, *Nanoscale*, 2011, **3**, 2511–2516.

43 M. Moxey, A. Johnson, O. El-Zubir, M. Cartron, S. S. Dinachali, C. N. Hunter, M. S. M. Saifullah, K. S. L. Chong and G. J. Leggett, Fabrication of Self-Cleaning, Reusable Titania Templates for Nanometer and Micrometer Scale Protein Patterning, *ACS Nano*, 2015, **9**, 6262–6270.

44 J. L. Hutter and J. Bechhoefer, *Rev. Sci. Instrum.*, 1993, **64**, 1868–1873.

45 D. F. Ogletree, R. W. Carpick and M. Salmeron, Calibration of Frictional Forces in Atomic Force Microscopy, *Rev. Sci. Instrum.*, 1996, **67**, 3298–3306.

46 M. Varenberg, I. Etsion and G. Halperin, An improved wedge calibration method for lateral force in atomic force microscopy, *Rev. Sci. Instrum.*, 2003, **74**, 3362–3367.

47 F. Zenhausen, M. Adrian, B. T. Heggeler-Bordied, L. M. Eng and P. Descouts, *Scanning*, 1992, **14**, 212–217.

48 A. Marti, G. Hähner and N. D. Spencer, Sensitivity of frictional forces to pH on a nanometer scale: a lateral force microscopy study, *Langmuir*, 1995, **11**, 4632–4635.

